Journal of Achievements in Materials and Manufacturing Engineering
VOLUME 15
ISSUE 1-2
March-April
2006

Optimisation of compound pressure cylinders

G.H. Majzoobi*, A. Ghomi
Faculty of Engineering, Mechanical Engineering Department,
Bu-Ali Sina University, Hamadan, Iran
* Corresponding author: E-mail address: gh_majzoobi@yahoo.co.uk

Received 15.11.2005; accepted in revised form 15.02.2006

Analysis and modelling

ABSTRACT

Purpose: The purpose of this paper is optimization of the weight of compound cylinder for a specific pressure. The variables are shrinkage radius and shrinkage tolerance.
Design/methodology/approach: SEQ technique for optimization, the finite element code, ANSYS for numerical simulation are employed to predict the optimized conditions. The results are verified by testing a number of closed end cylinders with various geometries, materials and internal pressures.
Findings: The weight of a compound cylinder could reduce by 60% with respect to a single steel cylinder. The reduction is more significant at higher working pressures. While the reduction of weight is negligible for $k<2.5$, it increases markedly for $2.5<k<5.5$. The stress at the internal radii of the outer and inner cylinders become equal to the yield stresses of the materials used for compound cylinders. The experimental results showed higher bursting pressure for optimized cylinders
Research limitations/implications: The research must be done for non-linear material models and for multiple compound cylinders
Practical implications: The results can be used for high pressure vessels such as artillery tubes, gun barrels and son on.
Originality/value: The numerical results indicated that for an optimum condition, the stress at the internal radii of the outer and inner cylinders become equal to the yield stresses of the materials used for compound cylinders.
Keywords: Numerical techniques; Compound cylinder; Optimisation; Finite element method

1. Introduction

Due to the ever-increasing industrial demand for axisymmetric pressure vessels which have had wide applications in chemical, nuclear, fluid transmitting plants, power plants, gas storages [1,2] and military equipments, the attention of designers has been concentrated on this particular branch of engineering. On the other hand, the increasingly scarcity of materials and higher costs have led researchers not to confine themselves to the customary elastic regime but attracted their attention to the elastic-plastic along with optimization approach which offer more efficient use of materials.

Basically there are two basic different elastic-plastic techniques to increase the pressure capacity of thick-walled cylinders. In the first, the cylinder is subjected to internal pressure so that its wall becomes partially plastic. The pressure is then released and the resulting residual stresses increase the pressure capacity of the cylinder in the next loading stage. This procedure is called 'autofrettage' [3,4]. The analysis of residual stresses and deformation in an autofrettaged thick-walled cylinder has been given by Chen [5] and Franklin and Morrison [6]. In the second technique, two or more cylinders are shrunk into each other with different diametral interferences to form a compound cylinder. The shrinkage produces a residual stress distribution within the walls of the cylinders, which improves the cylinder behavior against the working pressure [3].

In the second technique which is investigated in this work, two parameters are very important and must be selected carefully. These are: the shrinkage radius, c, and the diametral interference, Δ. Suppose that two cylinders are shrunk together. The inner and outer radii are $r_i = a$ and $r_o = c$, for the internal cylinder and $r_i = c$ and $r_o = b$ for the external cylinder, respectively. c is called the shrinkage radius.

The stress distribution across the wall of a cylinder is shown in figure 1. As the figure indicates, hoop and radial stresses decrease in a non-linear fashion from the inner surface toward the outer surface of the cylinder.

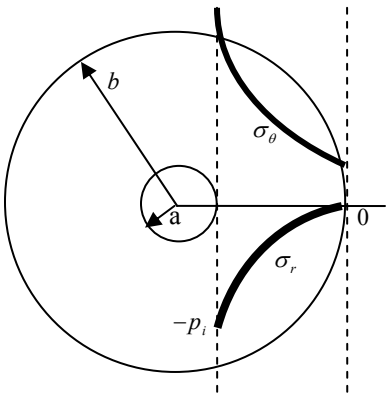

Fig. 1. Stress distribution for a cylinder under internal pressure

Dimensions and material of the cylinder are usually designed to tolerate the stresses which occur in the inner surface of the cylinder. On the other hand, as figure 1 indicates, the stresses reduce sharply towards the outer surface. This implies that the cylinder can partially be replaced by a lower strength and preferably lighter material to reduce the overall weight of the cylinder. For example, a steel cylinder can be partially replaced by aluminum. This necessitates that two cylinders are shrunk into each other forming a compound cylinder. However, as a result of shrinking, stress redistribution may occur across the wall of the compound cylinder. The stress redistribution is strongly influenced by shrinking radius (the outer radius of the inner cylinder and the inner radius of the outer cylinder) and diametral interference (shrink fit). The main objective of this work is to optimize the values of these two parameters so that the minimum weight for the compound cylinder is achieved.

Majzoobi *et al* [7] have shown that the best shrinkage radius can be obtained for k=2.2, when both the internal radii of the compound cylinder experience the same level of von-Mises equivalent stress. This can be predicted from the variation of maximum von-Mises stress versus shrinkage radius using a finite element code such as ANSYS without resorting to expensive and time-consuming experiments. They also have shown that the ideal diametral interference is obtained when the pressure produced by shrinking on the mating cylinder surfaces attains the value of pressure limit P_{yI}. Therefore, having known the value of P_{yI}, diametral interference can be estimated.

In the present work, the optimization techniques, numerical simulation and experiments are employed to predict the optimized conditions of a compound cylinder for a specific working pressure. SEQ technique is used for optimization purposes. The finite element code, ANSYS is employed for numerical simulations and finally, the results are verified by testing a number of closed end cylinders with various geometries, materials and internal pressures.

2. Analytical relations

2.1. Single cylinder

As stated earlier, an elasto-plastic behavior has been designated in this work. The model, shown in figure 2 is described as follows:

$$\sigma = \sigma_y + E^p \varepsilon \tag{1}$$

In which σ is the effective stress, σ_y is the initial yield stress, E^p is slope of the strain hardening segment of stress-strain curve, and ε is the effective strain.

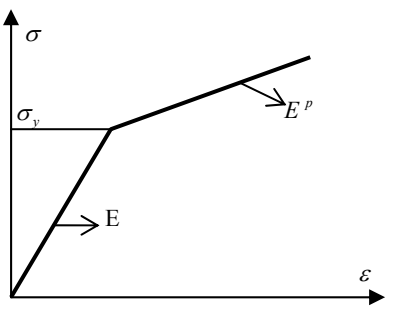

Fig. 2. Bi-linear stress-strain curve

Two pressure limits, P_{y1} and P_{y2} are considered to be of importance in study of pressurized cylinders. P_{y1} is the pressure required at the onset of yielding which occurs at the inner surface of the cylinder. The magnitude of P_{y1} based on von-Mises yield criterion is [3]:

$$P_{y1} = \frac{\sigma_y}{\sqrt{3}}\left(1 - 1/k^2\right) \quad \text{For open ends cylinder} \tag{2}$$

$$P_{y1} = \frac{\sigma_y}{\sqrt{3}} \frac{(k^2 - 1)}{\left(k^4 + 1/3\right)^{1/2}} \text{ For closed ends cylinder} \tag{3}$$

In which k is the ratio of outer to inner radii of the cylinder, k=b/a. The pressure P_{y2} is sufficient to bring the outer surface of

the cylinder to yielding. For an elastic perfectly plastic material, and according to Tresca yield criterion, P_{y2} is [3]:

$$P_{y2} = \sigma_y Ln(k) \tag{4}$$

When the pressure lies between P_{y1} and P_{y2}, the wall of cylinder becomes partially plastic (see figure 3). In this case, the distribution of radial and hoop stresses within the elastic region and plastic core can be described as follow:

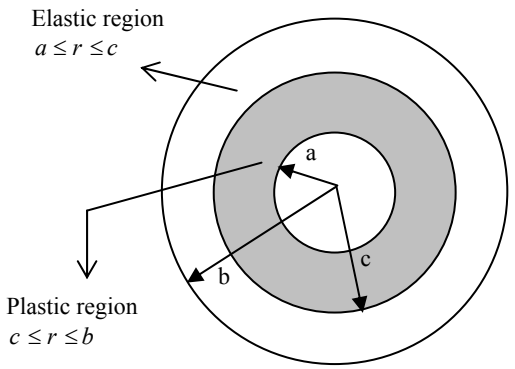

Fig. 3. Elasto-plastic regions in the wall of a single cylinder

For elastic perfectly plastic material:

In elastic region, $a \le r \le c$, for an external pressure P_0 and an internal pressure P_i :

$$\sigma_r = \frac{k^2 p_o - p_i}{1-k^2} - \frac{p_o - p_i}{1-k^2}\left(\frac{b}{r}\right)^2 \tag{5}$$

$$\sigma_\theta = \frac{k^2 p_o - p_i}{1-k^2} + \frac{p_o - p_i}{1-k^2}\left(\frac{b}{r}\right)^2 \tag{6}$$

For elastic-plastic material with linear strain hardening:

In plastic region, $c \le r \le b$, for an internal pressure P_i :

$$\sigma_r = -\frac{\sigma_y}{2}\left[\left(1-\frac{c^2}{b^2}\right) + \ln\frac{c^2}{r^2} + (1-\nu^2)\frac{E^p}{E}\left(\frac{c^2}{r^2} - \frac{c^2}{b^2}\right)\right] \Big/ \left[1 + (1-\nu^2)\frac{E^p}{E}\right] \tag{7}$$

$$\sigma_\theta = \frac{\sigma_y}{2}\left[\left(1+\frac{c^2}{b^2}\right) - \ln\frac{c^2}{r^2} + (1-\nu^2)\frac{E^p}{E}\left(\frac{c^2}{r^2} + \frac{c^2}{b^2}\right)\right] \Big/ \left[1 + (1-\nu^2)\frac{E^p}{E}\right] \tag{8}$$

If elasto-plastic boundary reaches the outer surface of the cylinder, i.e. the wall of cylinder becomes fully plastic (c=b), then the relations 7 & 8 reduce to:

$$\sigma_r = -\frac{\sigma_y\left[2\ln\frac{b}{r} + (1-\nu^2)\frac{E^p}{E}\left(\frac{b^2}{r^2} - 1\right)\right]}{2\left[1 + (1-\nu^2)\frac{E^p}{E}\right]} \tag{9}$$

$$\sigma_\theta = \frac{\sigma_y\left[2 - 2\ln\frac{b}{r} + (1-\nu^2)\frac{E^p}{E}\left(\frac{b^2}{r^2} + 1\right)\right]}{2\left[1 + (1-\nu^2)\frac{E^p}{E}\right]} \tag{10}$$

2.2. Compound cylinder

When two cylinders are shrunk together, a pressure, P_t, is produced at the contact surface of cylinders. This pressure for an elastic shrinkage is [3]:

$$P_c = \Delta \Big/ c\left[\frac{1}{E_2}\left(\frac{k_2^2+1}{k_2^2-1} + \upsilon_2\right) + \frac{1}{E_1}\left(\frac{k_1^2+1}{k_1^2-1} - \upsilon_1\right)\right] \tag{11}$$

In which Δ is diametral interference and c is the shrinkage radius. Subscripts '1' and '2' correspond to the inner and outer cylinders, respectively. Also, when the compound cylinder is subjected to a working pressure, a reacting pressure is developed at the contact surface of the mating cylinders and is given by [8,9]:

$$P_t = \frac{2P_i}{\left(k_1^2-1\right)\left[\frac{k_1^2+1}{k_1^2-1} + \frac{E_1}{E_2}\frac{k_2^2+1}{k_2^2-1} - \upsilon_1 + \frac{E_1}{E_2}\upsilon_2\right]} \tag{12}$$

These two systems of pressures act as external pressures for the inner cylinder and as internal pressures for the outer cylinder. Therefore, the stresses due to the working pressure and the contact pressure are superimposed to give the overall stress distribution across the wall of compound cylinder.

Generally, when two cylinders are shrunk together, the wall of both internal and external cylinders becomes partially plastic. Therefore, the relations of stress distribution across the wall of cylinders for elastic region and plastic core are introduced in this section. The inner cylinder is affected by two pressure systems:

$$P_i = P_w, \quad P_o = P_c + P_t \tag{13}$$

In which P_w is the working pressure, P_c is the pressure developed due to the shrinkage of the cylinders, and P_t is the reacting pressure at the contact surfaces of the cylinders due to the working pressure. The outer cylinder undergoes the following systems of pressure:

$$P_o = 0, \quad P_i = P_c + P_t \tag{14}$$

Now, each stress component in compound cylinder can be expressed as follows:

$$\sigma = \sigma' + \sigma'' \tag{15}$$

In which σ' is the stress due to the working pressure and σ'' is the stress induced by the contact pressures P_c and P_t. These two stresses can be calculated using equations 5 and 6. With the above considerations, the stress distribution in the wall of compound cylinder can be expressed as follow [8,9]:
For the inner cylinder:

$$\sigma_{r1}=\frac{1}{k_1^2-1}\left[P_i\left(1-\frac{c^2}{r^2}\right)-P_t\left(k_1^2-\frac{c^2}{r^2}\right)\right]-\frac{P_c}{k_1^2-1}\left(k_1^2-\frac{c^2}{r^2}\right) \tag{16}$$

$$\sigma_{\theta 1}=\frac{1}{k_1^2-1}\left[P_i\left(1+\frac{c^2}{r^2}\right)-P_t\left(k_1^2+\frac{c^2}{r^2}\right)\right]-\frac{P_c}{k_1^2-1}\left(k_1^2+\frac{c^2}{r^2}\right) \tag{17}$$

For the outer cylinder:

$$\sigma_{r2}=\frac{P_t}{k_2^2-1}\left(1-\frac{b^2}{r^2}\right)+\frac{P_c}{k_2^2-1}\left(1-\frac{b^2}{r^2}\right) \tag{18}$$

$$\sigma_{\theta 2}=\frac{P_t}{k_2^2-1}\left(1+\frac{b^2}{r^2}\right)+\frac{P_c}{k_2^2-1}\left(1+\frac{b^2}{r^2}\right) \tag{19}$$

When the mating cylinders in a compound cylinder become fully plastic, the stresses can be evaluated from the relations given below [10 & 11].
For the inner cylinder:

$$\begin{aligned}\sigma_{r1}=&\frac{\sigma_{y1}\left(\frac{b^2}{r^2}-1\right)\left[2\ln(k_1)+(1-\nu_1^2)\frac{E_1^p}{E_1}\left(k_1^2-1\right)\right]}{2\left(k_1^2-1\right)\left[1+(1-\nu_1^2)\frac{E_1^p}{E_1}\right]}\\&-\frac{P_i\left(\frac{b^2}{r^2}-1\right)}{k_1^2-1}-\frac{(P_t+P_c)\left(k_1^2-\frac{b^2}{r^2}\right)}{k_1^2-1}\\&-\frac{\sigma_{y1}\left[2\ln\frac{b}{r}+(1-\nu_1^2)\frac{E_1^p}{E_1}\left(\frac{b^2}{r^2}-1\right)\right]}{2\left[1+(1-\nu_1^2)\frac{E_1^p}{E_1}\right]}\end{aligned} \tag{20}$$

$$\begin{aligned}\sigma_{\theta 1}=&\frac{-\sigma_{y1}\left(\frac{b^2}{r^2}+1\right)\left[2\ln(k_1)+(1-\nu_1^2)\frac{E_1^p}{E_1}\left(k_1^2-1\right)\right]}{2\left(k_1^2-1\right)\left[1+(1-\nu_1^2)\frac{E_1^p}{E_1}\right]}\\&+\frac{\sigma_{y1}\left[2-2\ln\frac{b}{r}+(1-\nu_1^2)\frac{E_1^p}{E_1}\left(\frac{b^2}{r^2}+1\right)\right]}{2\left[1+(1-\nu_1^2)\frac{E_1^p}{E_1}\right]}\\&+\frac{P_i\left(\frac{b^2}{r^2}+1\right)}{k_1^2-1}-\frac{(P_t+P_c)\left(k_1^2+\frac{b^2}{r^2}\right)}{k_1^2-1}\end{aligned} \tag{21}$$

For the outer cylinder:

$$\begin{aligned}\sigma_{r2}=&\frac{\sigma_{y2}\left(\frac{d^2}{r^2}-1\right)\left[2\ln(k_2)+(1-\nu_2^2)\frac{E_2^p}{E_2}\left(k_2^2-1\right)\right]}{2\left(k_2^2-1\right)\left[1+(1-\nu_2^2)\frac{E_2^p}{E_2}\right]}\\&-\frac{\sigma_{y2}\left[2\ln\frac{d}{r}+(1-\nu_2^2)\frac{E_2^p}{E_2}\left(\frac{d^2}{r^2}-1\right)\right]}{2\left[1+(1-\nu_2^2)\frac{E_2^p}{E_2}\right]}\\&-\frac{(P_t+P_c)\left(\frac{d^2}{r^2}-1\right)}{k_2^2-1}\end{aligned} \tag{22}$$

$$\begin{aligned}\sigma_{\theta 2}=&\frac{-\sigma_{y2}\left(\frac{d^2}{r^2}+1\right)\left[2\ln(k_2)+(1-\nu_2^2)\frac{E_2^p}{E_2}\left(k_2^2-1\right)\right]}{2\left(k_2^2-1\right)\left[1+(1-\nu_2^2)\frac{E_2^p}{E_2}\right]}\\&+\frac{\sigma_{y2}\left[2-2\ln\frac{d}{r}+(1-\nu_2^2)\frac{E_2^p}{E_2}\left(\frac{d^2}{r^2}+1\right)\right]}{2\left[1+(1-\nu_2^2)\frac{E_2^p}{E_2}\right]}\\&+\frac{(P_t+P_c)\left(k_2^2+\frac{d^2}{r^2}\right)}{k_2^2-1}\end{aligned} \tag{23}$$

According to Tresca yield criterion, the equivalent stress σ_{eq} can be defined as:

$$\sigma_{eq}=\sigma_\theta-\sigma_r \tag{24}$$

If the cylinder is intended to remain elastic throughout the loading process of the cylinder, then the equivalent stress should not exceed the yield stress of the material, i.e.:

$$\sigma_{eq}=\sigma_\theta-\sigma_r\le\sigma_y \tag{25}$$

Radial displacement across the wall of the cylinder is obtained from the relation [7]:

$$u=\frac{r}{2G}\left[(1-\nu)\sigma_y\left(\frac{c}{r}\right)^2+(1-2\nu)\sigma_r\right] \tag{26}$$

3. Optimization problem definition

In the optimization problem, the variables vector is defined as:

$$(X)=(x_1 \quad x_2 \quad x_3 \quad x_4)^T$$

In which $x_1=a$ is the inner radius of the internal cylinder, $x_2=c$ is the shrinkage radius (the outer radius of the inner cylinder or the inner radius of the external cylinder), $x_3=b$ is the outer radius of the external cylinder and finally, $x_4=\Delta$ is the diametral interference. The objective function, $f(x)$, is the weight of compound cylinder. The constraints of the problem are defined as follow:

1- $g_1(X)=\sigma_{eq}\big|_{r=x_1}-\sigma_{y1}\le 0$. This implies that equivalent stress in the inner radius of the internal cylinder should not exceed the yield stress, σ_{y1}.

2- $g_2(X)=\sigma_{eq}\big|_{r=x2}-\sigma_{y2}\le 0$. This implies that equivalent stress in the inner radius of the external cylinder should not exceed the yield stress, σ_{y2}.

3- $g_3(X)=u_r\big|_{r=x1}-u_a\le 0$. This is an optional constraint implying that the radial displacement at the inner radius of compound cylinder must remain less than a specific value, u_a.

4- x_1 and x_2 have always to be less than x_2 and x_3, respectively.

5- x_1 and x_3, i.e. the inner and outer radii of compound cylinder, are forced to remain within the range $a_1\le x\le a_2$.

The optimization problem can be summarized as follows:

Minimize: $f(x)=\pi\cdot\gamma_1\cdot\left(x_2^2-x_1^2\right)+\pi\cdot\gamma_2\cdot\left(x_3^2-x_2^2\right)$ Subject to:

$$g_1(x_1,x_2,x_3,x_4)=\sigma_{eq}\big|_{r=x1}-\sigma_{y1}\le 0$$
$$g_2(x_1,x_2,x_3,x_4)=\sigma_{eq}\big|_{r=x2}-\sigma_{y2}\le 0$$
$$g_3(x_1,x_2,x_3,x_4)=u_r\big|_{r=x1}-u_a\le 0$$
$$g_4(x_1,x_2,x_3,x_4)=a_1-x_1\le 0$$
$$g_5(x_1,x_2,x_3,x_4)=x_1-x_2\le 0$$
$$g_6(x_1,x_2,x_3,x_4)=x_2-x_3\le 0$$
$$g_7(x_1,x_2,x_3,x_4)=x_3-a_2\le 0$$

Where γ_1 and γ_2 are the specific weights of the inner and outer cylinders, respectively.

SQP technique [10,11] was employed for optimization process which was performed using MATLAB software.

For elaso-plastic optimization, the constraints 1 and 2 must be redefined as follow:

$$g_1(X)=\sigma_{eq}\big|_{r=x_1}-\alpha\sigma_{y1}\le 0$$
$$g_2(X)=\sigma_{eq}\big|_{r=x2}-\beta\sigma_{y2}\le 0$$

In which α and β are greater than 1 and must be provided by the user.

4. Material and specimens

Two materials, aluminum and steel were used in this investigation. The stress-strain curves of the materials were obtained from a number of tensile tests using the universal testing machine, Instron. The stress-strain curves for aluminum and steel alloys are shown in figures 4 and 5, respectively. The material's properties obtained from the figures are summarized in Table 1.

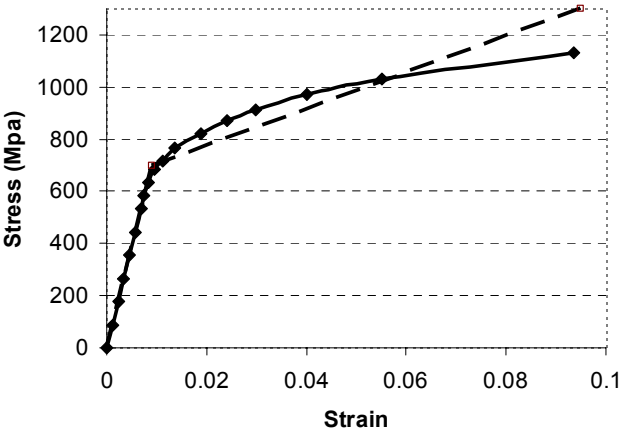

Fig. 4. Stress-strain curve for steel alloy

Table 1

	$\sigma_y\,(Mpa)$	$E\ (GPa)$	$E^P\,(GPa)$	ν
Al.	90	72	1.75	0.33
St.	700	207	4.5	0.29

As the figures suggest, the non-linear portions of the curves have been fitted with a linear approximation the slope of which, E^p, is given in Table 1.

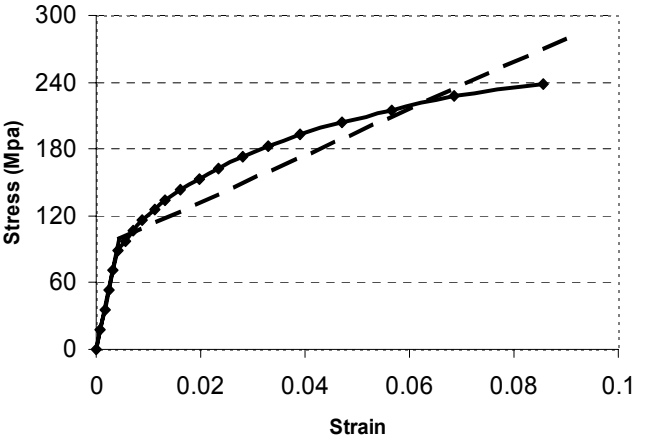

Fig. 5. Stress-strain curve for aluminum alloy

Figure 6 illustrates the shape of the specimens tested in this work. The shapes of specimens were adopted from the work of Manning [12 & 13]. Dimensions of the specimens were the same as those obtained from the optimization of the compound cylinders. However, the gauge length of the cylinders was 150 mm and remained constant for all specimens.

Fig. 6. The external and internal cylinders before testing and one specimen after bursting

5. Optimization results

5.1. Single-metal compound cylinder

In this section, the two mating cylinders are assumed to be made of the same material which is either steel or aluminum. The optimization is performed using the optimizing problem defined in previous section. Having known the value of the outer radius (or the inner radius) of the compound cylinder, the other variables, $x_1 = a$ (or $x_3 = b$), $x_2 = c$ and $x_4 = \Delta$ are calculated. The results for various working pressures are given in Table 2 for aluminum cylinders and in Table 3 for steel cylinders.

The results are also graphically shown in figures 7 & 8 for aluminum and steel cylinders, respectively. It can be deduced from the figures that, as the working pressure increases, k=a/b decreases and diametral interference, Δ increases.

Table 2
Optimum values for aluminum compound cylinder (a=0.01m)

P_i (Mpa)	b(m)	k	c(m)	Δ mm	c/b	W (kg/m)
30	0.0144	1.44	0.012	0.0043	0.833	0.91
35	0.0154	1.54	0.0124	0.0053	0.805	1.16
40	0.0166	1.66	0.0129	0.0065	0.777	1.49
45	0.018	1.80	0.0134	0.0077	0.744	1.90
50	0.0197	1.97	0.014	0.0091	0.711	2.44
55	0.0218	2.18	0.0145	0.0106	0.665	3.18
56	0.022	2.20	0.0148	0.0110	0.673	3.26

Table 3
Optimum values for steel compound cylinder (a=0.01m)

Pi (Mpa)	b(m)	k	c(m)	□mm	c/b	W (kg/m)
250	0.0148	1.48	0.0121	0.0125	0.818	2.94
300	0.0162	1.63	0.0128	0.0169	0.788	4.05
350	0.018	1.80	0.0134	0.0208	0.744	5.52
400	0.0202	2.02	0.0141	0.0253	0.698	7.60
433	0.022	2.20	0.0148	0.0296	0.673	9.47

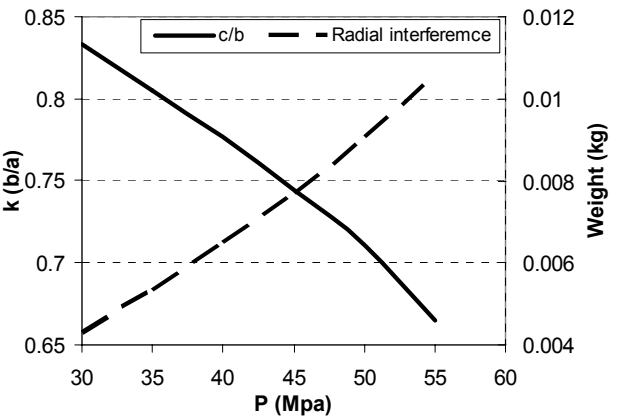

Fig. 7. Variation of k and Δ vs. working pressure for aluminum compound cylinder

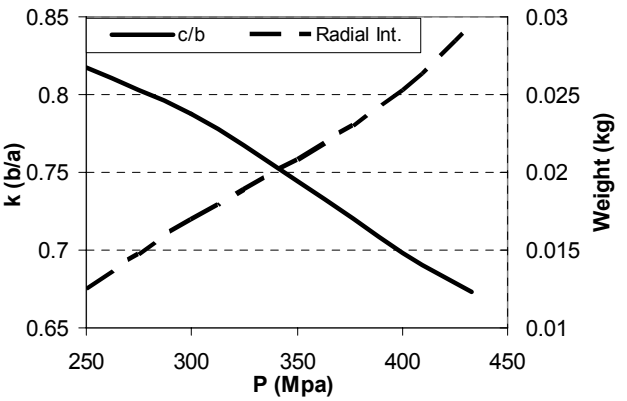

Fig. 8. Variation of k and Δ vs. working pressure for steel compound cylinder

5.2. Bi-metal compound cylinders

The optimization of bi-metal compound cylinders is the main objective in this work. Again, having assumed a value for outer radius of cylinder, the other variables are obtained using the optimizing problem defined in section 4. Some typical results are given in Table 4 and graphically shown in figure 9.

Table 4
Optimum values for aluminum-steel compound cylinder

			b=0.016			
P_i (Mpa)	a(m)	k	c(m)	Δ mm	c/b	Weight
150	0.0126	1.27	0.0142	0.0104	0.888	2.40
160	0.0123	1.30	0.0141	0.0108	0.881	2.58
170	0.0121	1.32	0.0139	0.0114	0.869	2.70
180	0.0119	1.34	0.0138	0.0120	0.863	2.82
190	0.0117	1.37	0.0137	0.0127	0.856	2.94
			b=0.019			
Pi (Mpa)	a(m)	k	c(m)	Δ mm	c/b	Weight
150	0.0149	1.28	0.0168	0.0121	0.884	3.43
160	0.0147	1.29	0.0167	0.0131	0.879	3.57
170	0.0144	1.32	0.0165	0.0136	0.868	3.79
180	0.0141	1.35	0.0164	0.0142	0.863	4.00
190	0.0138	1.38	0.0162	0.0147	0.853	4.21
			b=0.022			
Pi (Mpa)	a(m)	k	c(m)	Δ mm	c/b	Weight
150	0.0173	1.27	0.0195	0.0142	0.886	4.56
160	0.017	1.29	0.0193	0.0150	0.877	4.81
170	0.0167	1.32	0.0191	0.0158	0.868	5.06
180	0.0163	1.35	0.019	0.0164	0.864	5.38
190	0.016	1.38	0.0188	0.0172	0.855	5.62
190	0.0165	1.33	0.019	0.0145	0.864	5.22

The figure illustrates the variation of normalized c (c/b) versus a (b/a=k) for different values of working pressure. This is a useful diagram as, having known the value of working pressure, the figure can provide the optimum values of c and a.

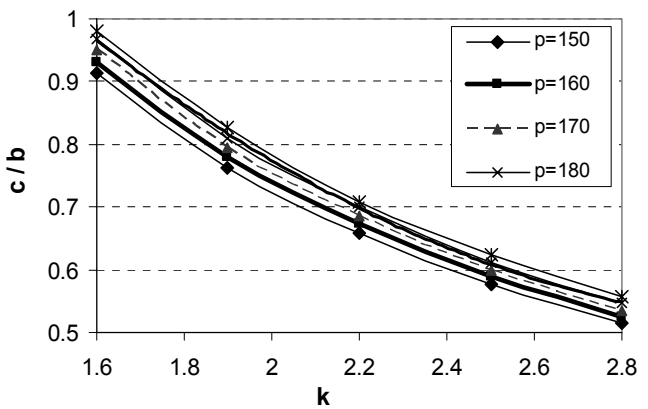

Fig. 9. variation of (c/b) versus k for different values of working pressure

The variation of the weight of cylinder versus working pressure for a single steel and steel-aluminum compound cylinder is illustrated in figure 10. As the figure suggests, as far as the weight of the cylinder is concerned, the difference between a single and a compound cylinder becomes more significant at higher pressures. The percent of weight reduction versus k is depicted in figure 11.

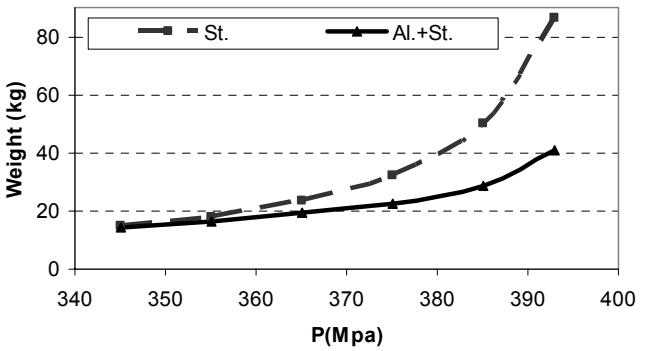

Fig. 10. Variation of the weight of single and compound cylinders versus internal pressure ratio k

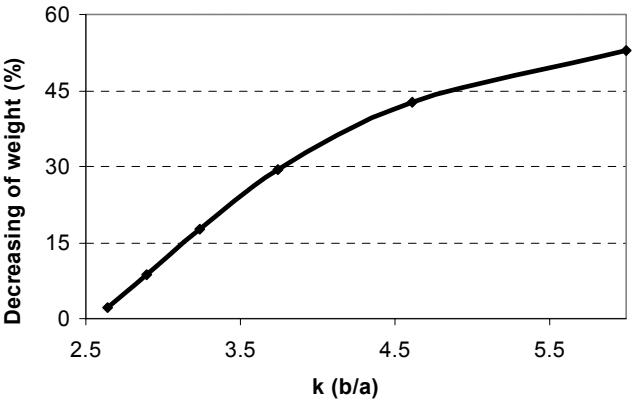

Fig. 11. The rate of weight reduction for compound cylinder versus k

It can be deduced from the figure that while, the reduction of weight is negligible for the values of k<2.5, for 2.5<k<5.5 increases markedly and thereafter begins to flat out.

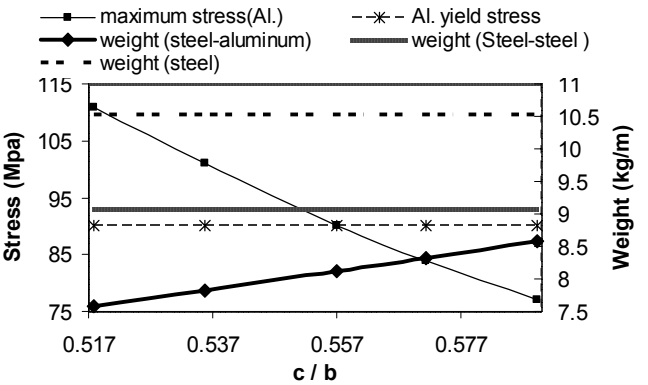

Fig. 12. Variation of maximum stress in aluminum cylinder and the weight versus c/b for three types of cylinders

In figure 12, the variation of maximum stress in aluminum cylinder and the weight versus c/b for three types of cylinder, steel single, steel-steel compound and aluminum-steel compound are compared. The figure compares the results for the optimized conditions, a=0.01m, c=0.056m, b=0.028m, Δ =0mm, $p_i = 190MPa$, with non-optimized conditions. As the figure shows, the optimum value of c/b is located at the intersection of maximum stress and weight graphs. The figure clearly illustrates the superiority of aluminum-steel compound cylinder with respect to the other two types of cylinders.

In figure 13, maximum stress and the weight of steel (inner cylinder) are plotted against c/a. As the figure suggests, the maximum stress in inner cylinder diminishes and the weight rises as c/a increases. The two curves intersect at the optimum point, c/a=2.52. This point corresponds to the optimum state, a=0.02 m, c=0.0491m, b=0.08m, Δ =0.02574, $p_i = 320MPa$.

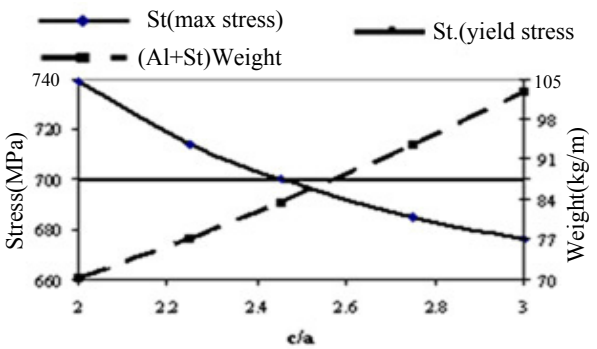

Fig. 13. Variation of maximum stress and the weight of steel (inner cylinder) against c/a

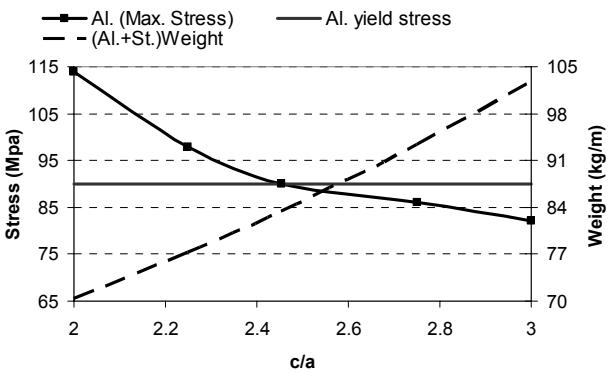

Fig. 14. Variation of maximum stress and the weight of aluminum (outer cylinder) against c/a

A similar diagram for aluminum (outer cylinder) is drawn in figure 14. As the figure indicates, the maximum stress in outer cylinder diminishes and the weight rises as c/a increases. The two curves intersect at the optimum point, c/a=2.52.

As stated in section 1, elasto-plastic regime can increase the pressure capacity of compound cylinders. In this work, steel-steel compound cylinders were autofrettaged before applying an internal working pressure. The results are compared with those obtained for a steel-steel compound cylinder without autofrttage in figure 15. The optimization problem is the same as that defined in section 4. The hoop and radial stress distribution are given by equations 20 to 23. It can be seen in figure 15 that the weight of the autofrettaged compound cylinder is significantly higher than that for non-autofrettaged cylinders.

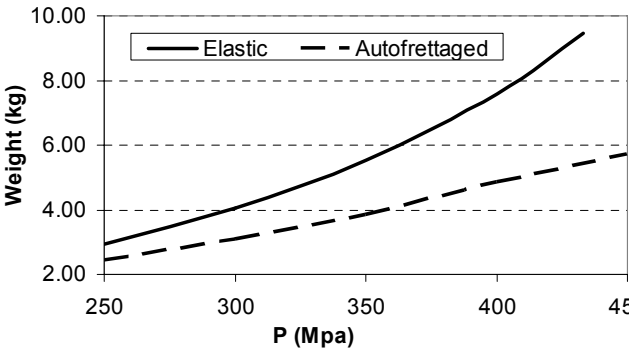

Fig. 15. The effect of autofrettage on the weight of compound cylinders

6. Numerical simulations

The finite element predictions were obtained using the elastic-plastic module of the ANSYS finite element code. An axisymmetric finite element mesh using second order quadrilateral elements were used, as shown in figure 16. In the numerical simulations, kinematic hardening with $\beta = 0$ was considered for the material model [14]. It is evident that the Bauchinger effects are very important in analysis of thick-walled cylinders which are subjected to reversed loadings [14]. On the other hand, β =1 corresponds to a state of pure isotropic hardening. A kinematic/isotropic hardening is defined by a value of β between 0 and 1. The value of β can be estimated from a reversed loading test. From a number of tension-compression tests, the materials were found to be pure kinematic hardened ($\beta = 0$).

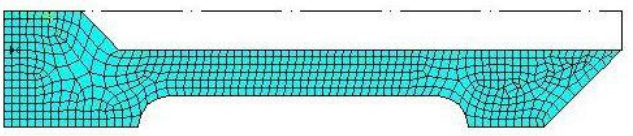

Fig. 16. A finite element model of the compound cylinder

Numerical simulations of aluminum compound cylinders were carried out using the optimized variables given inTable 2: a=0.01 m, c=0.0148 m ,b=0.022 m and Δ =0.011 mm.

The von-Mises stress distribution across the wall of the cylinder is shown in figure 17. As the figure suggests, internal radii of the inner and outer cylinders experience the same level of von-Mises equivalent stress which is exactly equal to the yield stress of the material used for the simulations. This verifies the results given by Majzoobi et al [7] as described in section 1.

When a variable violates its optimum value, the stress at the internal radii would be no longer the same. A typical example of the state of stress for non-optimized condition is illustrated in figure 18. The figure clearly shows that for a slightly different value of c (c=0.014 m), the stress distribution becomes quite different from the optimized conditions.

Numerical simulations of steel compound cylinders were carried out using the optimized variables given in Table 3: a=0.0165 m ، c=0.019 m , b=0.022 m و Δ=0.0145 mm.

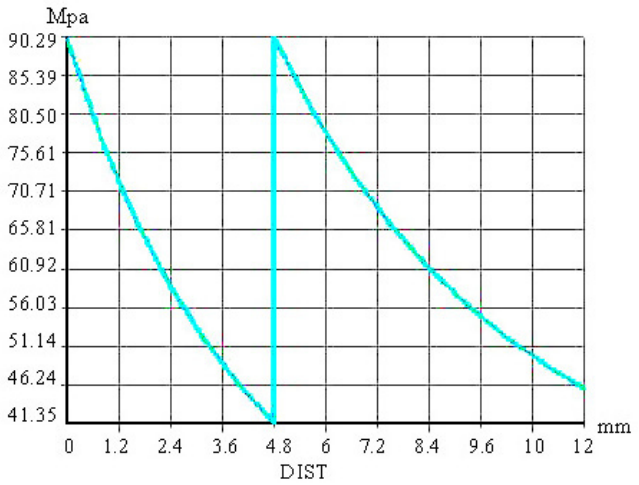

Fig. 17. von-Mises stress distribution in aluminum alloy compound cylinder for optimized conditions. a=0.01 m, c=0.0148 m ,b=0.022 m and Δ =0.011 mm

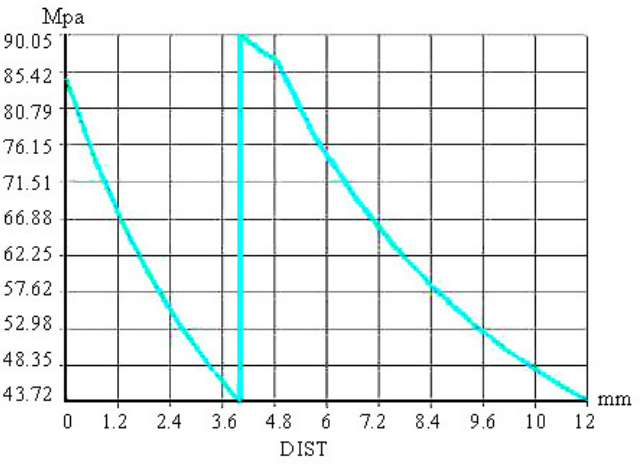

Fig. 18. von-Mises stress distribution in aluminum alloy compound cylinder for non-optimized conditions. a=0.01 m ، c=0.014 m , b=0.022m and Δ =0.011 mm

The von-Mises stress distribution across the wall of the cylinder is shown in figure 19. Again, as observed for aluminum cylinders , the figure suggests that, internal radii of the inner and outer cylinders experience the same level of von-Mises equivalent stress, exactly equal to the yield stress of the steel alloy used for the simulations. A typical example of the state of stress for non-optimized condition is illustrated in figure 20. The figure clearly shows that for a slightly different value of c (c=0.0195 m), the stress distribution becomes quite different from the optimized conditions

Numerical simulations of aluminum-steel compound cylinders were carried out using the optimized variables given in Table 4: a=0.02 m ، c=0.0491 m , b=0.08 m و Δ=0.0257 mm.

The von-Mises stress distribution across the wall of the cylinder is shown in figure 21. The results shown in the figure are quite consistent with those given for aluminum and steel cylinders in figures 17 and 19. As seen in the figure, von-Mises stress at the inner radii of steel (inner cylinder) and aluminum (outer cylinder) is equal to the yield stress of steel ($\sigma_y = 700MPa$) and the yield stress of aluminum (σ_y $90MPa$), respectively.

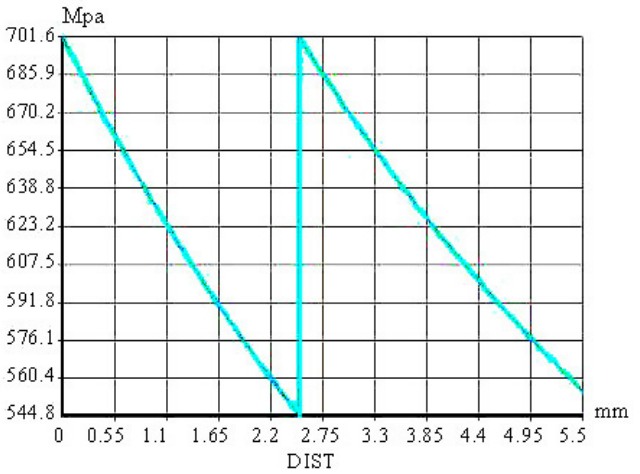

Fig. 19. von-Mises stress distribution in steel alloy compound cylinder for optimized conditions. a=0.0165 m ، c=0.019 m , b=0.022 m و Δ=0.0145 mm

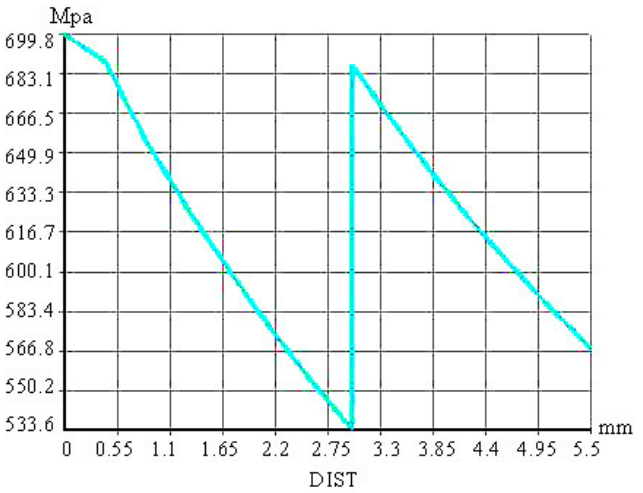

Fig. 20. von-Mises stress distribution in steel alloy compound cylinder for non-optimized conditions.. a=0.0165 m ، c=0.0195m , b=0.022 m و Δ =0.0145 mm

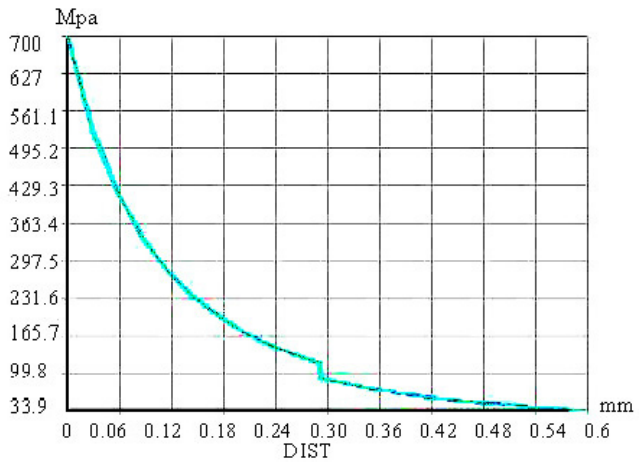

Fig. 21. von-Mises stress distribution in aluminum- steel compound cylinder for optimized conditions. a=0.02 m ، c=0.0491 m , b=0.08 m و Δ=0.0257 mm

Again, a typical example of the state of stress for non-optimized condition is illustrated in figure 22. It can be seen in the figure that for a slightly different value of c (c=0.058 m), the stress distribution becomes quite different from the optimized conditions, i.e. von-Mises stress at the inner radii of compound cylinder is less than the yield stresses of steel and aluminum cylinders.

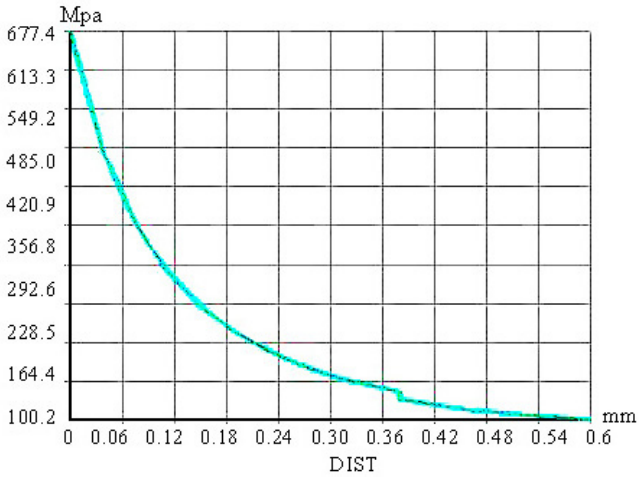

Fig. 22. von-Mises stress distribution in aluminum- steel compound cylinder for non-optimized conditions. a=0.02 m ، c=0.058 m , b=0.08 m و Δ=0.0257 mm

7. Experimental results

The experiments were carried out using a high pressure pump with a pressure capacity ranging from 1 to 40000 psi. The diag gauge of the pump had a minimum division of 500 psi. Therefore an error of about $\pm 250 psi$ was expected for each reading. The dimensions of the specimens and the bursting pressure for aluminum-aluminum compound cylinders are given in Table 6. The specimens's geometry was already shown in figure 5. Two of the specimens (the first two rows of the table) have the optimum values provided in section 5. For the other specimens, a, b and Δ were kept constant and the value of the shrinkage radius, c, was varried.

Table 6
Bursting pressure of optimized and non-optimized cylinders

Specim. NO.	a (mm)	c (mm)	b (mm)	Δ (mm)	P_{burst} (psi)
Optimum (case 1)	10	14.9	22	0.0022	8000
Optimum (case 2)	10	14.8	22	0. 022	8000
3	10	13.5	22	0. 022	7500
4	10	14	22	0. 022	7900
5	10	15.5	22	0. 022	7000
6	10	16.6	22	0. 022	5000

As can be seen from the table, the maximum bursting pressure has been attained for the optimized dimmensions while, for non-optimized states the bursting pressure is considerable lower with respect to the optimized conditions.

In order to avoid the paper to become lenghtly, the results for other cylinders, steel-steel and alumium steel compound cylinders are not given here.

8. Conclusions

From the optimization, numerical and experimental results the following conclusion can be derived:

1. High pressure cylinders can partially be replaced by a lower, lighter and cheaper material to reduce the cost and weight of cylinders.
2. The weight of a compound cylinder could reduce by 60% with respect to its equivalent single steel cylinder for the same working pressure.
3. The difference between a compound cylinder and its equivalent single cylinder becomes more significant at higher working pressures.
4. While, the reduction of weight is negligible for the values of k<2.5, it increases markedly for 2.5<k<5.5 and thereafter begins to flat out.
5. The numerical results indicated that for an optimum condition, the stress at the internal radii of the outer and inner cylinders become equal to the yield stresses of the materials used for compound cylinders. For the compound cylinders made of a single material, both the internal radii of the compound cylinder experience the same level of von-Mises equivalent stress.
6. A number of cylinders with the optimized and non-optimized dimensions were pressurized to burst. The experimental results also showed higher bursting pressure for optimized cylinders.
7. The weight of autofrettaged compound cylinders is significantly higher than that for non-autofrettaged cylinders.

Acknowledgements

The authors wish to thank Dr Maleki, the Dean of Fcaculty of Engineering, Bu-Ali Sina University for his support. They also like to thank Mr. Heidari for his contribution in preparation of specimens and conducting the experiments.

References

[1] E. David, An overview of advanced materials for hydrogen storage, Journal of Material Processing Technology, vol. 162-163, pp. 169-177, 2005.

[2] H.H. Lee, J.H. Yoon, J.S. Park, Y.M. Yi, A study of failure characteristic of spherical pressure vessels, Journal of Material Processing Technology, vol. 164-165, pp. 882-888, 2005.

[3] T.Z. Blazinski, Applied elasto-plasticity of solids, Hong-Kong, Macmillan, 1983.

[4] GH Majzoobi, GH Farrahi, AH.Mahmoudi, A finite element simulation and an experimental study of autofrettage for strain hardened thick-walled cylinders, J. Mater. Sci. Eng. A., vol. 359, pp. 326-31, 2003.

[5] PCT. Chen, Stress and deformation analysis of autofrettaged high pressure vessels, ASME special publication 110, PVP. New York, ASME United Engineering Center; pp. 61-7, 1986.

[6] GJ Franklin, JLM. Morrison, Autofrettage of cylinders: prediction of pressure, external expansion curves and calculation of residual stresses, Proceeding of institute of Mechanical Engineers, vol. 174, pp. 947-74, 1960.

[7] G. H. Majzoobi, G. H. Farrahi, M. K. Pipelzadeh and A. Akbari, Experimental and Finite Element Prediction of Bursting Pressure in Compound Cylinders, International Journal of Pressure Vessels and piping , vol. 81, pp 889-896, 2004.

[8] A. Ghomi, Optimum Design of thick-walled pressure cylinders (in Persian), MS.c final project, Bu-Ali SIna University, Hammadan, Iran, 2005.

[9] A. R. Ragab, S. E. Bayomi, Engineering Solid Mechanics, Fundamentals and Applications. Boca Raton CRC press, 1998.

[10] Garret N. Vanderplaats, Numerical Optimization Techniques for Engineering Design with Applications, McGraw-Hill, New York, 1989.

[11] Edgard Himmelblan, Optimization of Chemical Processes, McGraw-Hill, 1989.

[12] WRD. Manning, Labrow S. High pressure engineering. London: CRC Press; 1971.

[13] WRD. Manning, Bursting pressure as the basis for cylinder design, Trans ASME, Journal of Pressure Vessel Technology, vol. 100, pp. 374-81, 1978.

[14] P.C.T.Chen, The Bauschinger and hardening Effect on Residual Stresses in an Autofrettaged Thick-Walled Cylinder, Journal of Pressure Vessel Technology, vol. 108, pp. 108-112, 1986.